Research Article

Buthenia Abd Al hamza Hasoon, Bassam Shaker Mahmood, Erieg Abdulwahab Mohamed, Majid Sakhi Jabir, Kareem Hussein Jawad, Nehia Neama Hussein, Ghassan Mohammad Sulaiman*, Yaser Hassan Dewir*, and Nóra Mendler-Drienyovszki

Tangerine fruit peel extract mediated biogenic synthesized silver nanoparticles and their potential antimicrobial, antioxidant, and cytotoxic assessments

https://doi.org/10.1515/gps-2024-0126
received June 06, 2024; accepted September 03, 2024

Abstract: The utilization of plant bioactive composites has concerned substantial attention due to their possible use in the development of novel antibiotics, containing the environmentally sustainable synthesis of nanoparticles. In the current study, a green and eco-friendly process was employed to synthesize silver nanoparticles (Ag-NPs) and to evaluate their anti-bacterial, anti-oxidant, and anti-cancer potentials. The characterization of the Ag-NPs involved UV-vis spectroscopy, Fourier-transform infrared spectroscopy (FTIR), energy-dispersive X-ray spectroscopy (EDX), X-ray diffraction (XRD), field emission scanning electron microscopy (FESEM), and transmission electron microscopy (TEM). The UV-vis spectrum of Ag-NPs was 437 nm. The FTIR absorption peaks detected at 685.48 cm^{-1} confirmed their characteristics. The FESEM displayed that Ag-NPs have an average size of 30 nm. The TEM revealed that the Ag-NPs have an irregular spherical shape with 16 nm size distribution. The XRD results provided a strong indication that the green synthesized Ag-NPs was of high purity with crystalline nature. The anti-bacterial properties were investigated at different concentrations for both the ethanolic tangerine peel extract and Ag-NPs. The results of anti-bacterial activity showed that 100 $\mu g \cdot mL^{-1}$ was potent concentration, but the Ag-NPs were more effective than the ethanolic tangerine peel extract. For the ethanolic extract, the inhibition zone was 17.50 ± 0.20 mm for *K. pneumoniae* and 14.40 ± 0.20 mm for *B. cereus*. For the Ag-NPs, the inhibition zone was 25.50 mm for *K. pneumoniae* and 20.50 mm for *B.* cereus. Furthermore, the antioxidant examination revealed more potent free radical scavenging activity of the Ag-NPs than the ethanolic peel extract alone. The ethanolic extract ranged 46–77% while the Ag-NPs ranged 57–88%. Additionally, the anti-proliferative of the Ag-NPs against the lung cancer cell line (A549) was more potent than the ethanolic extract alone. The cytotoxic activity was 90.03% and 78.50%, respectively. The anti-proliferative effect of Ag-NPs is attributed to cell death, induced apoptosis, and enhanced generation of reactive oxygen species. Our findings highlight the potential and further utilization of Ag-NPs in medicinal applications particularly for cancer therapeutics.

Keywords: Ag-NPs, antibacterial, antioxidant, anticancer, apoptosis, ROS

*** Corresponding author: Ghassan Mohammad Sulaiman,** Department of Applied Sciences, University of Technology, Baghdad, Iraq, e-mail: ghassan.m.sulaiman@uotechnology.edu.iq
*** Corresponding author: Yaser Hassan Dewir,** Plant Production Department, College of Food and Agricultural Sciences, King Saud University, Riyadh, 11451, Saudi Arabia, e-mail: ydewir@ksu.edu.sa
Buthenia Abd Al hamza Hasoon: Department of Applied Sciences, University of Technology, Baghdad, Iraq, e-mail: Buthenia.h.hasoon@uotechnology.edu.iq
Bassam Shaker Mahmood: Department of Applied Sciences, University of Technology, Baghdad, Iraq, e-mail: 11654@uotechnology.edu.iq
Erieg Abdulwahab Mohamed: Department of Applied Sciences, University of Technology, Baghdad, Iraq, e-mail: erige.a.mohamed@uotechnology.edu.iq
Majid Sakhi Jabir: Department of Applied Sciences, University of Technology, Baghdad, Iraq, e-mail: 100131@uotechnology.edu.iq
Kareem Hussein Jawad: Department Laser Engineering, University of Technology, Baghdad, Iraq, e-mail: Kareem.h.jawad@uotechnology.edu.iq
Nehia Neama Hussein: Department of Applied Sciences, University of Technology, Baghdad, Iraq, e-mail: 100103@uotechnology.edu.iq
Nóra Mendler-Drienyovszki: Research Institute of Nyíregyháza, Institutes for Agricultural Research and Educational Farm (IAREF), University of Debrecen, P.O. Box 12, 4400, Nyíregyháza, Hungary, e-mail: mendlerne@agr.unideb.hu

1 Introduction

The synthesis of nanoparticles (NPs) has an area of intense investigation due to their unique physical and chemical

properties and wide range of applications in various fields, for instance, drug, catalysis, and microelectronics. Usually, NPs have been synthesized by physical and chemical approaches, which often include the usage of toxic chemicals, high temperatures, and energy-intensive actions [1]. However, the rising concern for environmental sustainability has led to the examination of more ecofriendly methods, i.e., green synthesis of NPs [2]. Green synthesis refers to the fabrication of NPs by natural, renewable, and biodegradable precursors, often derived from plants, microbes, or other biological bases [3]. Green synthesis typically includes mild reaction conditions, usages non-toxic reagents, and generates minimal waste produces. Conventional physical and chemical approaches for NP synthesis can be energy intensive, generate dangerous by-products, and rely on the usage of harsh chemicals [4]. Synthesis of Ag-NPs offer significant therapeutic and biological possible [1]. Their ecofriendly synthesis by plant extracts is a supportable option and endows them with unique biological actions [5]. The continued exploration of their properties and optimization of their formulations will pave the way for advanced therapeutic solutions and innovative applications in medicine and environmental science. The hypothesis for the green synthesis of NPs by plant extracts typically revolves about the idea that plant extracts can act as reducing, capping, scalability, and stabilizing mediators [6]. As compared to physical and chemical approaches, green synthesis offers some advantages. It often uses renewable and readily available natural resources as forerunners, reducing the need on non-renewable and possibly toxic chemicals. Additionally, the mild reaction conditions, for instance room temperature and atmospheric pressure, require less energy input, making the process more sustainable [7]. The biologically resulting capping and stabilizing agents used in green synthesis can enhance the bio-compatibility and stability of the resulting NPs [8]. Despite these benefits, green synthesis also has some tests. The synthesis procedure can be more compound and less controlled than the traditional approaches, leading to differences in NP size, shape, and possessions [9]. In contrast to bulk materials, a significant proportion of the physical and chemical properties of NPs are substantially influenced by their size. Besides, inorganic NPs have single features due to their small size and large surface-to-mass ratio. Varied kinds of metallic NPs have been prepared, such as gold (Au) and Ag-NPs that have gained substantial care due to their high exhibition in many practical fields, e.g., optics, bio-sensing, and catalysis [10]. *Geranium* leaf extract was used to create Ag-NPs by the fast reduction of silver ions in an aqueous silver nitrate solution. The particles produced quasilinear superstructures ranging from 16 to 40 nm size, which were observed by transmission electron microscopy (TEM) and found to be very stable and crystalline [11]. Singh et al. [12,13] employed *Panax ginseng* leaf and root extract to produce Au-NPs and Ag-NPs using medicinal plants as sources of raw materials and their biological activities. Saifuddin et al. [14] reported a novel combinational synthesis strategy for the creation of Ag-NPs using a combination of culture supernatant of *B. subtilis* and microwave irradiation in water. It should be noted that some investigations have demonstrated the toxicity of Ag-NPs in respect to cells, including those involving rat hepatocytes and neuronal cells, mouse stem cells, and human lung epithelial cells [15–18]. Utilizing both *in vitro* and *in vivo* models, the research on toxicity is crucial in this regard [19]. Consequently, the mechanisms of Ag-NPs production by plants and their interactions are the focus of our study, which leads to the numerous applications of Ag-NPs. Ag-NPs have been used as an excellent antibacterial for hastening some chemical reactions [20]. A possibly viable approach includes producing Ag-NPs from green synthesis and mixing them with extracts that are biologically benign [21]. Plant extracts cover a variety of bioactive composites, for instance, phenolics, alkaloids, terpenoids, flavonoids, and proteins, which can efficiently decrease metal ions to form NPs. These phytochemicals provide stabilization and capping, important for the development of NPs with shapes and sizes. Thus, the use of plant extracts can replace conventional chemical methods, reducing environmental and health hazards associated with NP synthesis. The organic synthesis of NPs by plant extracts signifies an important progression over physical and chemical approaches. It offers an ecofriendly, maintainable, and cost-effective approach, with improved bio-compatibility and scalability [1,22–24]. The use of plant extracts, such as tangerine peel, exemplifies the potential of utilizing natural resources and agricultural waste for high-value NP production, aligning with the principles of green chemistry and sustainability. Tangerines are small, easy-to-peel citrus fruits that are native to China and South Asia. They have a deep orange color, a sweet citrusy taste, and are packed with nutrients that can benefit our health in many ways [25]. Tangerine peels are rich in a naturally super-flavonoid, or antioxidant that possesses numerous pharmacological properties that are beneficial to human health [26]. These properties include anti-oxidation and anti-inflammatory effects [27]. Tangerine peel contains a variety of bioactive compounds such as flavonoids, phenolics, and essential oils [28]. The special ability of tangerine fruit peel lies in its unique combination and high concentration of specific bioactive compounds, such as hesperidin, naringin, tangeritin, and limonene, coupled with its rich polysaccharide content, and it simply acts as a readily available natural resource [29]. These compounds are known for their reducing and capping properties, which are essential for the synthesis of NPs, offering advantages in terms of stability,

biological activity, and sustainability [30]. Citrus species belong to the family Rutaceae and constitute some of the most commercially important crops grown in tropical and subtropical climates [31]. Citrus peel is an important raw material for producing oils that are essential. Such oils have been used by humans since prehistoric times. Today, these oils are used in the scents, food, and beverage. Similarly, these oils have been used in folk and traditional remedies [32].

Ag-NPs have been utilized in large scale in many applications in biomedicine such as new antimicrobial mediators, nanomaterials for tissue regeneration and repair, coatings for biomaterials and medical devices, drug delivery system, platforms for detection and diagnosis for cancers, and therapeutic alternatives with developed performance. Ag-NPs could potentially be utilized in cancer, antiviral, and antibiotic therapies. Furthermore, Ag-NPs are suitable for usage as additives in a broad range of medical equipment and components, such as membranes, dentures, dental implants, and bone cement hydrogels, bases, broken bones, and catheters, to prevent or lessen the growth of biofilm or other pathogenic microorganisms, as well as to encourage and hasten the process of gum, wound, and bone growth healing [33]. The prevalence of antibiotic resistance is a persistent problem as a result of the body developing an effective resistance to antibiotics [34]. Consequently, in order to combat resistant microbial infections, it is imperative to utilize and create novel inhibitory substances. In this regard, the current work demonstrates that ethanolic peel extract was employed as an agent to the biosynthesis of Ag-NPs. Ethanolic peel extract and Ag-NPs were used to investigate the antibacterial, antioxidant, and anticancer potential *in vitro*.

2 Experimental methods

2.1 Chemicals materials

Silver NP was synthesized from high-purity silver nitrate ($AgNO_3$, 98% purity at 1 mM, sourced from Sigma Aldrich). The tangerine plant peel used in this research was collected from local market. Muller–Hinton agar (MHA) and nutrient broth (NB) medium were obtained via Hi-Media, India. DPPH stain utilized in the study were obtained from Acino-Pharma AG. Ascorbic acid, and DPPH were obtained by Sigma-Aldrich. Antibiotic disks were obtained from Liofilchem, Roseto degli Abruzzi, Italy.

2.2 Preparation of the plant extract

The peel of the tangerine plant employed in this study was sourced from a local market. The plant's peel was subsequently subjected to a drying process at room temperature for several days, followed by grinding. A quantity of 150 g of the plant's peel was carefully placed within a wide weave cotton canvas bag, which was then inserted into a Soxhlet apparatus for extraction. The extraction process involved the use of 850 mL of ethanol (70%) and extended over a period of 7 h distributed across three days. The resulting extract was then spread out on a glass plate and allowed to dry in an oven. Subsequently, the dried extract was collected using a blade and transferred into a tube. The preparation of the extract entailed weighing 1 g of the plant extract, softening it in 10 mL of distilled water (100%), and conducting a series of decimal dilutions as required [22–24].

2.3 Synthesis of Ag-NPs

We weighed 0.034 mg of a 1 millimolar solution of silver nitrate, and dissolved it in 100 mL of distilled water. Subsequently, 90 mL of the silver nitrate solution were combined with 10 mL of plant extract (100% concentration). This mixture was subjected to heating in a water bath until a noticeable change in color occurred (Figure 1). A series of decimal dilutions was performed as necessary [23,24].

2.4 Characterization of Ag-NPs

UV Visible Spectroscopy (UV-1900, Shimadzu, Japan) was utilized to examine the spectral range of 200–800 nm [35]. The Fourier-transform infrared (FTIR) analysis was conducted using a Bruker instrument in Billerica, MA, USA, covering the range of 400–4,000 cm^{-1} to identify various functional groups [36]. The Department of Applied Sciences at the University of Technology, Iraq, conducted FTIR and UV-is investigations [37]. The shape and size distribution were investigated utilizing a German-made ZEISS LEO 912 AB TEM device [38]. A Shimadzu XRD-6000 diffractometer with Cu K radiation (0.154 nm) was employed for analyzing crystalline samples using X-ray diffraction (XRD), producing diffraction patterns between 20°C and 70°C [39]. Furthermore, field emission scanning electron microscopy (FE-SEM) analysis was conducted using a JEM-1400 instrument located in Peabody, MA, USA [40].

2.5 Microorganisms activation

The microorganisms used in antimicrobial assays, such as *K. pneumoniae* and *Bacillus cereus*, were utilized as

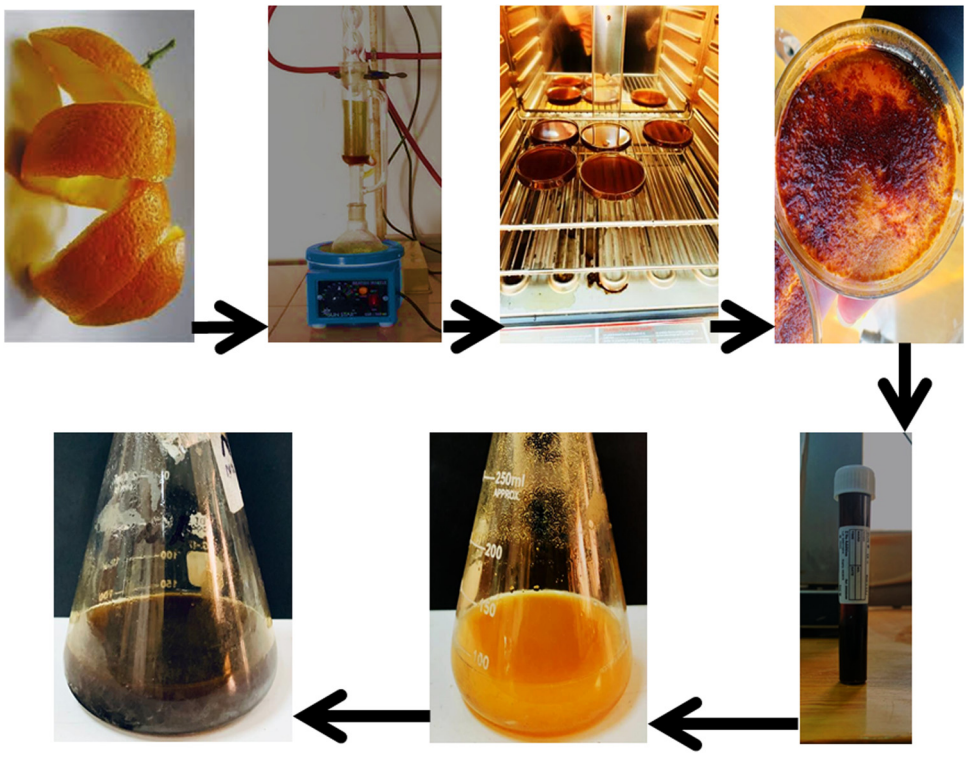

Figure 1: Steps for preparation of Ag-NPs mediated tangerine peel extract.

bacterial models. Microorganisms were activated by culturing them in Brain Heart Infusion agar and subsequently placing them in an incubator at 37°C for 24 h, followed by assessing the turbidity of bacteria by comparing it to the 0.4–0.5 McFarland standard. These microbial isolates were obtained from the Microbiology Laboratory within the Biotechnology Branch, Department of Applied Sciences, University of Technology, Iraq.

2.6 Anti-microbial assay

The assessment of the antimicrobial activity of tangerine peel extract and its conjugated Ag-NPs with ethanolic peel extract was conducted using the well-diffusion agar method. The four types of bacteria mentioned earlier were cultured using MHA for activation. Each inoculum was adjusted to the 0.5 McFarland standard and applied onto the surface of MHA using a sterilized cork borer, creating 5 mm wells in each plate. Subsequently, different concentrations (20, 40, 60, 80, 100 $\mu g \cdot mL^{-1}$) of the extract and NPs were added into each well, and the plates were then incubated at 37°C for 24 h. The inhibition zone was measured, and all experiments were conducted in duplicate [41].

2.7 Antioxidant activity

The DPPH radical activity was performed using the stated methodology [38,39]. The extract and the NPs were prepared by diluted in distilled water at various concentrations (20, 40, 60, 80, and 100 $\mu g \cdot mL^{-1}$). DPPH was prepared by dissolving 0.004 mg in 100 mL of ethanol. Ascorbic acid was prepared by adding 0.05 g to 100 mL of ethanol and water solution (1:1; v/v). Approximately 750 µL of DPPH were added to 750 µL of various concentrations of the extract and the NPs. The final volume was 1,500 µL and the reaction mixture was mixed and kept for 30 min at room temperature. The optical density (OD) was assessed at 517 nm. The samples' ability to block the DPPH was estimated using Eq. 1 [36,37]:

$$\text{Antioxidant activity\%} = \text{Control OD} - \text{Sample OD} / \text{Control OD} \times 100 \quad (1)$$

2.8 Cytotoxic activity

To determine the cytotoxic effect of synthesized Ag-NPs, cell culture medium (RPMI-1640) was used to maintain A549 cells, and supplemented with 10% Fetal Bovine

Serum, 100 units·mL^{-1} of Penicillin, and 100 g·mL^{-1} of Streptomycin. Trypsin-EDTA was employed to decease the cells. Twice a week, at 80% confluence, the cells were reseeded and were stored at 37°C [29]. Ag-NPs and MTT assay was used in 96-well plates. 1×10^4 of A549 cells were seeded per well. The cells were exposed to various concentrations of tested compound for 72 h. MTT stain of 28 µL of 2 µg·mL^{-1} was added to the sample. It was kept within 37°C for 2.5 h. 100 µL of dimethyl sulfoxide (DMSO) was added to the wells and kept at 37°C with shaking for 15 min. The measurement of absorbency (Abs.) were measured in triplicate using a microplate reader set to 492 nm [41,42]. The samples' ability to block the cytotoxic effect was estimated using Eq. 2 [43,44]:

$$\text{Cytotoxic effect\%} = \text{Abs. of control} - \text{Abs. of sample/Abs. of control} \times 100 \quad (2)$$

2.9 Measurement of lactate dehydrogenase (LDH) release

LDH investigation was performed according to the instructions of the manufacturer. Cells were cultured without the presence of phenol red marker. Next cells were treated with Ag-NPs at numerous concentrations (12.5, 25, 50, 100, and 200 µg·mL^{-1}) for a duration of 24 h. As a positive control, triton-X was employed. Samples were kept for 2 hours at 37°C. Once the time for incubation has elapsed, 75 µL of samples were moved to a new 96-well plate from every test and control well. Following that, 50 µL of the Cyto-Tox 96VR ingredient was mixed with each aliquot of the substance. The plate was kept at room temperature for 30 min and protected from light by foil. For 1 h, add 50 µL of the stopping solution. At optical density (OD) at 490 nm was measured. The results were determined using Eq. 3 [45–48].

$$\text{LDH release\%} = \text{OD Sample LDH release} / \text{OD Control LDH release} \times 100 \quad (3)$$

2.10 Acridine Orange@Ethidium Bromide (AO/EB)

The compound-induced death in A549 cells was evaluated through the application of the AO/EB (Sigma–Aldrich, USA) staining technique. A549 cells were seeded on 24-well plates, treated with Ag-NPs and plant extract at an IC_{50} concentration, and then allowed for incubation for a further 20 h. Two treatments of phosphate-buffered saline were carried out on the cells. For 2 min, the wells were then filled with an identical volume of cells and treated with 10 µL of double fluorescent dyes. Finally, a fluorescent microscope was employed to show the cells [49].

2.11 Determination of reactive oxygen species (ROS)

Utilizing a FACSCalibur flow cytometer, the making of ROS in cells was evaluated. On the six-well plates, SKOV-3 cells were placed at a cell density of 1×10^6. During an overnight keep period, cells received treatment for 10 h with Ag-NPs and plant extract at an IC_{50} level. After that, a new medium was added with ROS probes diacetyldichlorofluorescein (DCFH-DA) (15 µM) and kept for 30 min in the dark. A flow cytometer (BD Biosciences) was employed to determine the fluorescence intensity of the obtained cells [50–52].

2.12 Statistical analysis

With the use of Graph Pad Prism 6, the acquired data were analyzed statistically. For this investigation, the unpaired *t*-test was employed. The mean value ± standard deviation (SD) of three independent experiments are expressed [53].

3 Results and dissection

3.1 Phytofabrication of Ag-NPs

The production of Ag-NPs from plant extracts includes three stages. In the first stage, metal ions (Ag^+) are reduced to metal atoms (Ag°). In the second stage, small nearby Ag-NPs accumulate into bigger particles, increasing thermodynamic stability. In the third stage, the end of phase, defines the final morphology of the NPs (Figure 1). Plants are ideal for Ag-NPs synthesis because they contain a wide range of biomolecules, including flavonoids, terpenoids, and alkaloids, which operate as potent reducing agents, as noted by Sabry et al. [28].

3.2 Characterization of Ag-NPs

3.2.1 UV visible spectrophotometer

Using a UV visible spectrophotometer, the combination and stability of reduced Ag-NPs, which is in the form of

solution, were investigated. The absorbance increase was between 430 and 450 nm. Color change is one of the rapid and easily observable tests that indicate the formation of NPs. This color change is attributed to a phenomenon known as surface plasmon resonance (SPR). SPR involves the oscillation of conduction electrons at the surface of the NPs in resonance with the incident light. When Ag-NPs are formed, the interaction between the positive and negative charges on their surface results in distinctive absorption bands in the visible light spectrum, causing a visible color change in the solution. For instance, the formation of Ag-NPs typically results in a light-orange to dark-orange color shift due to SPR. SPR designs are frequently used as tests for the production of NPs, since SPR is dependent on a number of variables, for instance, size and substrate dielectric values [54]. The extracellular reduction of Ag^{+} ions indicated the production of Ag-NPs (Figure 2).

3.2.2 FTIR assay

The FTIR analysis of the Ag-NPs solution, which was reduced and covered with subordinate metabolites from tangerine peel, exhibited important absorption peaks at 3,527.97, 3,197.39, 2,049.41, 1,624.73, 1,358.81, and 685.48 $cm^{-1,}$ as seen in Figure 3. The presence of alkanes was indicated by the appearance of the absorption band at 3,197.39 cm^{-1} (C–H), while the band at 2,049.41 cm^{-1} confirmed the existence of alkynes. The absorption band at 1,624.73 cm^{-1} exposed the presence of N–C and N═C groups, and the presence of ═CH in aromatic compounds was indicated by the C–O group at 685.48 cm^{-1} in the biosynthesized Ag-NPs [55]. FTIR analysis of the Ag–NP solution revealed the presence of various functional groups, including alkanes, alkynes, N–C, N═C, and aromatic C–O groups. These findings suggest that the Ag-NPs were coated or capped by secondary

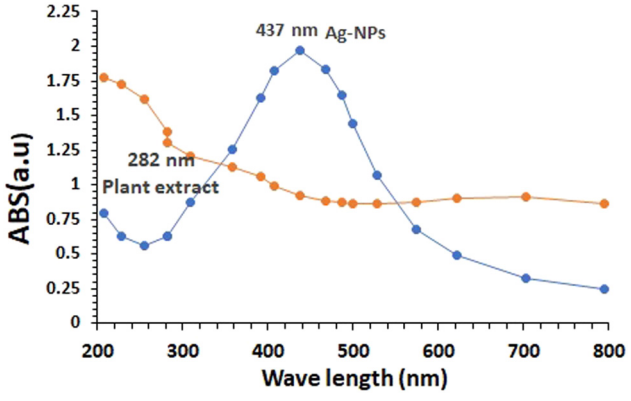

Figure 2: UV-vis for Ag-NPs synthesized by tangerine peel from 1 M solution of $AgNO_3$.

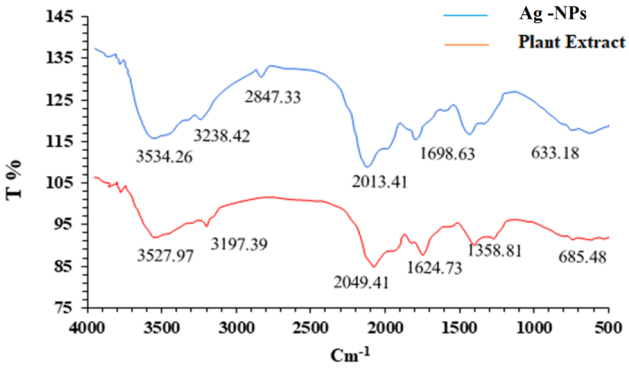

Figure 3: FTIR spectroscopy for Ag-NPs synthesized by Tangerine fruit peel extract.

metabolites from the tangerine peel extract used in the green synthesis. These results are in agreement with previous studies [56,57]. Elemental mapping was determined using energy-dispersive X-ray (EDX), and the elemental structures of Ag-NPs were examined. The Ag-NPs' EDX ranges reveal that the three primary elements in Figure 4 are Ag, oxygen (O), and potassium (K). Additionally, the amount of Ag was highest at 58.20%, O at 41.10%, and K at 0.70%.

3.2.3 FESEM assay

FESEM examination was carried out to study the surface shape and particle size of Ag-NPs. Figure 5 shows the FE-SEM image and particle size distribution of Ag-NPs. The size of the Ag-NPs, as observed in Figure 5a and b, was determined to be 30 nm. These images were captured as part of a study on Ag-NPs prepared using a green synthesis technique, which involved combining Ag-NPs with ethanolic extract. The results indicate that the Ag-NPs are coated with ethanolic peel extract, providing an encapsulating layer on the outside. This finding aligns with the results obtained from UV and TEM analysis. The TEM image of Ag-NPs was examined, along with a histogram displaying the particle sizes obtained from a set of TEM images. Measurements were performed on 100 particles using Image J program. These images were captured to study Ag-NPs prepared through a green synthesis method, which involved the combination of Ag-NPs and their bonding with ethanolic peel extract. Figure 6a demonstrates the TEM image of Ag-NPs in the form of an asymmetrical spherical particle. The average size of the Ag-NPs, as determined by the size distribution analysis, is approximately 16 nm, as depicted in Figure 6b. The FESEM and TEM results are consistent, confirming that synthesized Ag-NPs using the green method with ethanolic tangerine peel extract have an average size in the range of 16–30 nm and are coated/

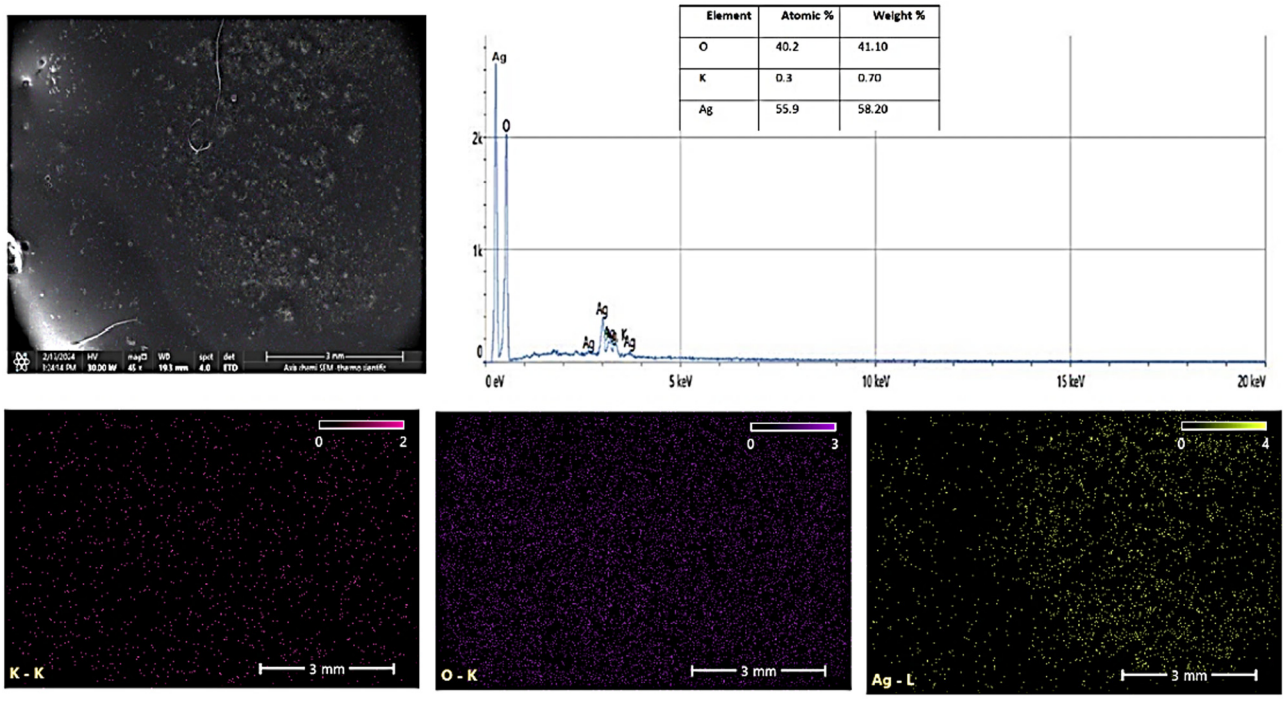

Figure 4: EDX and mapping of Ag-NPs.

capped by the extract components, forming a protective layer around the NPs.

3.2.4 X-ray diffraction (XRD) evaluation

The crystalline nature of Ag-NPs was further confirmed by XRD analysis (Figure 7). XRD is used to characterize the crystallographic structure, grain size, and preferred orientation in polycrystalline or powder solid samples. Ag-NPs display diffraction peaks at 2θ angles of 38.64°, 44.54°, 69.38°, and 78.28°, which are corresponding to levels (111), (200), (220), and (311) planes of face centered cubic (fcc) crystal, respectively [40,58]. Utilizing typical data (JCPDSile No. 84-0713; JCPDS No. 89-3722), every peak was properly matched with the hexagonal arrangement of Ag-NPs. After

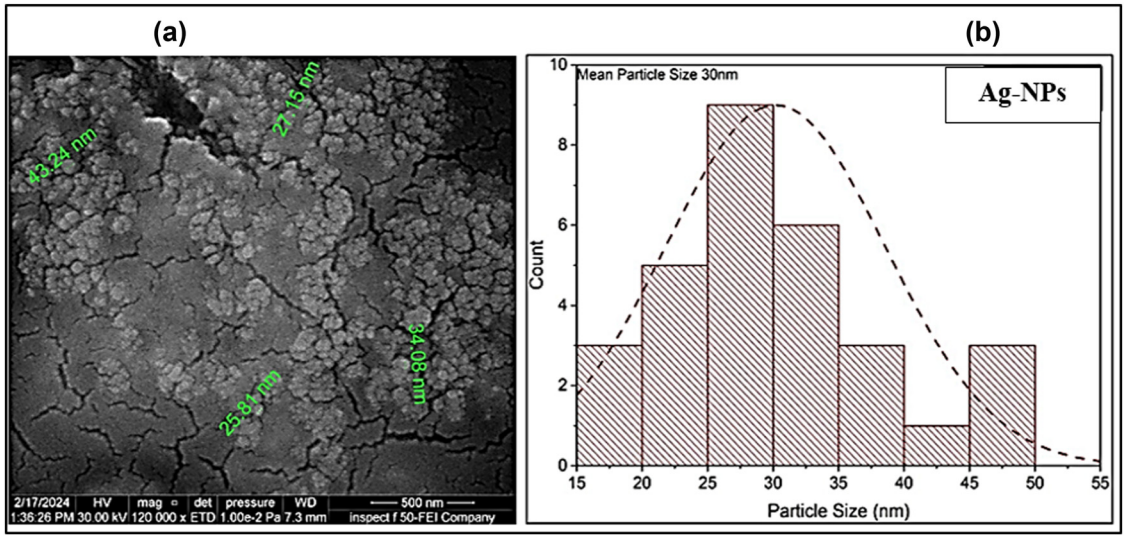

Figure 5: (a) FESEM image and (b) size distribution of Ag-NPs.

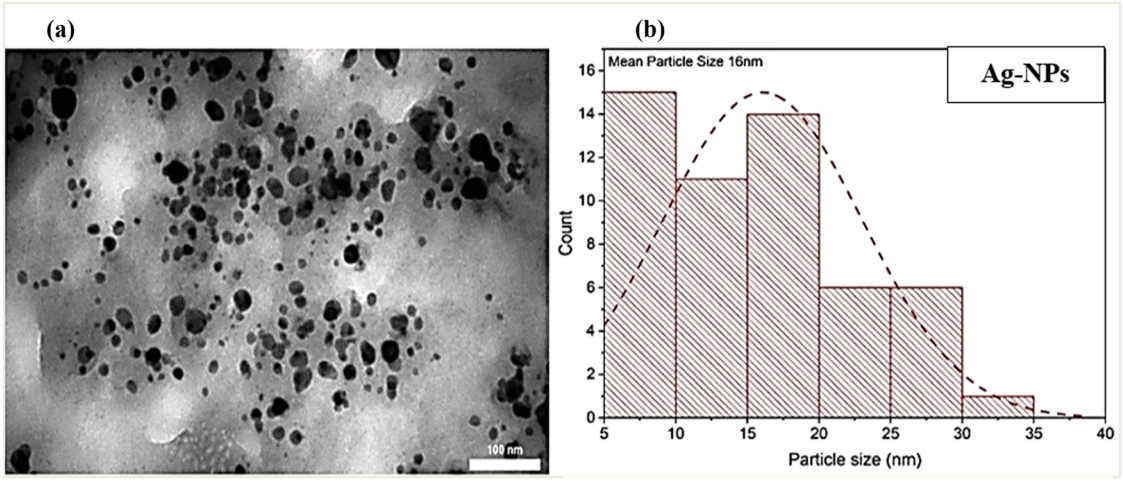

Figure 6: (a) TEM image of Ag-NPs. (b) Size distribution (Histogram).

5 min, we observed that the peaks' strength had dropped due to the ethanolic peel extract's reduction of silver ions by green synthesis. Following that, we are left with isolated Ag-NPs that are free of the other organic substances in the fluid. A fresh peak of NPs was seen to arise (Figure 7), revealing that the synthesized Ag-NPs are composed of pure crystalline silver and the particle size is approximately 33.5 nm. The peak corresponding to (111) plane is more intense than the other planes, suggesting that the (111) plane is in the predominant orientation. In addition, the pattern indicated that Ag-NPs were mainly present in the nanocomposites with no contamination peaks.

3.3 Antibacterial test

This study highlights the superior antibacterial properties of the tangerine peel-derived Ag-NPs compared to the ethanolic extract. The assay was conducted at concentrations (20, 40, 60, 80, and 100 μg·mL^{-1}) of the ethanolic extract and Ag-NPs against *K. pneumoniae* and *B. cereus*. The results showed that the antibacterial activities increased with increasing concentrations for both the ethanolic extract and Ag-NPs. The results showed highest inhibition zone on *K. pneumoniae* (17.50 ± 0.20 mm) and *B. cereus* (14.40 ± 0.20 mm) at a concentration of 100 μg·mL^{-1} for ethanolic

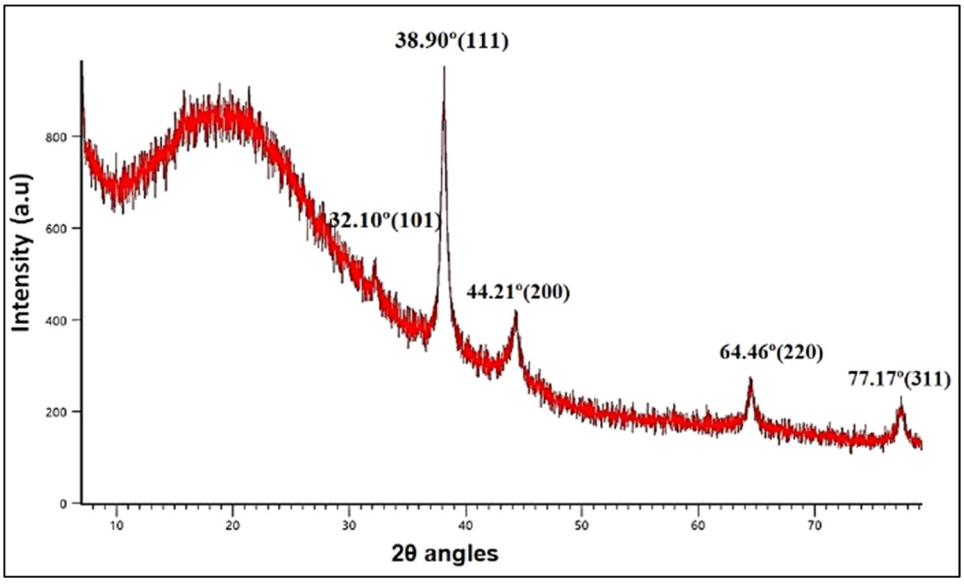

Figure 7: XRD for Ag-NPs synthesized by ethanolic extract from Tangerine peel.

Table 1: Anti-bacterial activity of Tangerine peel ethanolic extract

Microorganism	Inhibition zone of Tangerine peel ethanolic extract (mm) ± SD					
	Concentrations (μg·mL^{-1})					
	Control	20	40	60	80	100
K. pneumoniae	6.00 ± 0.01	15.50 ± 0.12	16.30 ± 0.03	16.40 ± 0.10	16.50 ± 0.21	17.50 ± 0.20
B. cereus	6.00 ± 0.01	7.66 ± 0.12	9.50 ± 0.03	9.60 ± 0.10	12.33 ± 0.21	14.40 ± 0.20

extract peel, as shown in Table 1 and Figure 8. While the highest inhibition zone on *K. pneumoniae* (25.50 mm) and *B. cereus* (20.50 mm) for the Ag-NPs at a concentration of 100 μg·mL^{-1} is shown in Table 2 and Figure 9. When we tested the antibacterial activity at concentrations of 20 μg·mL^{-1} and 40 μg·mL^{-1} of the ethanolic extract on *B. cereus*, the result was negative, but positive results were obtained when these concentrations were tested with Ag-NPs. The study under distilled water showed no zone of inhibition against the bacteria as shown in Figures 8 and 9. Therefore, in the present study, it is observed that the Ag-NPs synthesized by ethanolic extract of tangerine peel, exerted a significant antibacterial action against the tested bacteria. The zone of inhibition against tested bacteria for Ag-NPs is 25.50 mm which shows excellent antibacterial activity with large zone of inhibition. Our study concludes that Ag-NPs synthesized from tangerine peel extract have significant antibacterial action. Ag-NPs have demonstrated

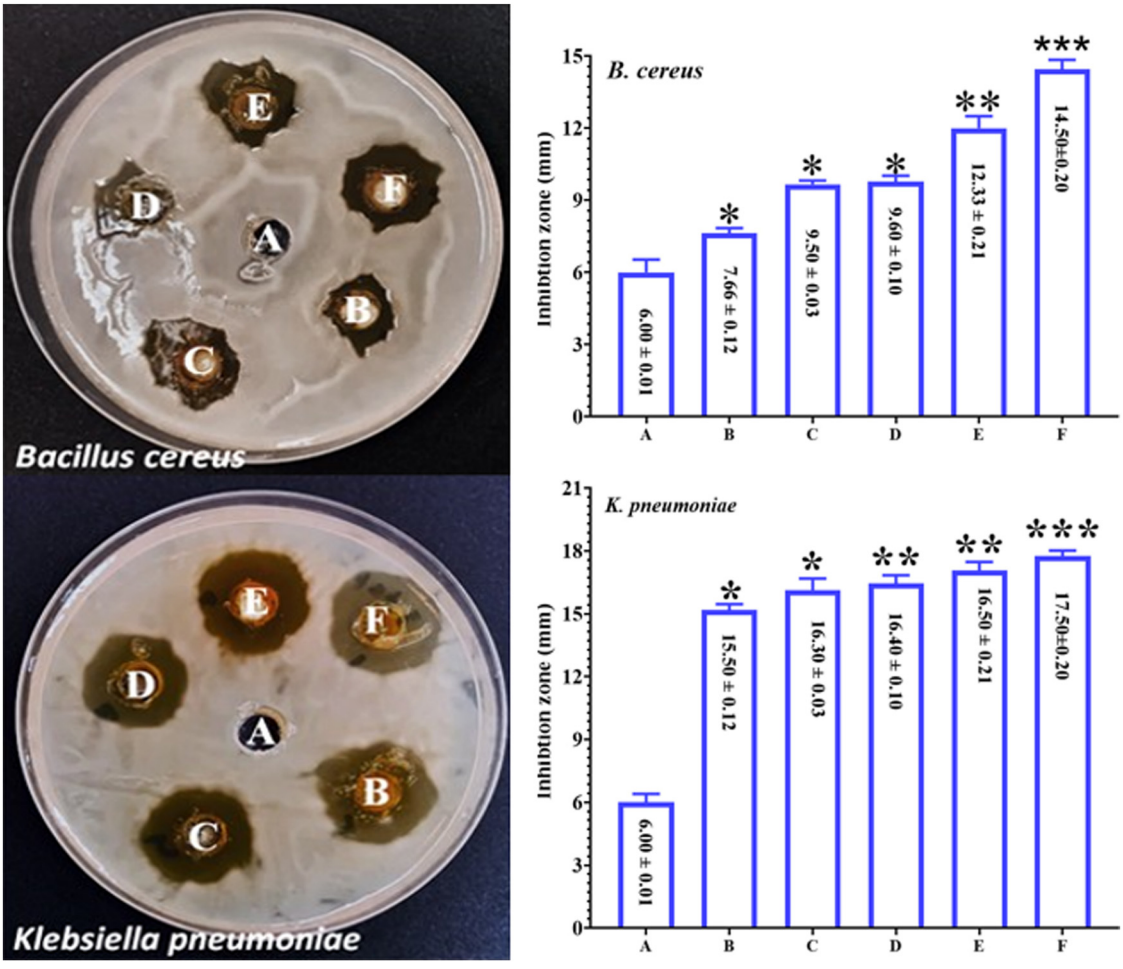

Figure 8: Antibacterial activity of peel extract against *K. pneumoniae* and *B. cereus*. *A* = control, (*B* = 20 μg·mL^{-1}, *C* = 40 μg·mL^{-1}, *D* = 60 μg·mL^{-1}, *E* = 80 μg·mL^{-1}, *F* = 100 μg·mL^{-1}). *P < 0.05, **P < 0.01, ***P < 0.001.

Table 2: Anti-bacterial activity of Ag-NPs

Microorganism	Inhibition zone of Ag-NPs (mm) ± SD					
	Concentrations (μg·mL^{-1})					
	Control	20	40	60	80	100
K. pneumoniae	6.00 ± 0.01	15.50 ± 0.03	18.80 ± 0.12	20.50 ± 0.10	22.50 ± 0.21	25.33 ± 0.20
B. cereus	6.00 ± 0.01	15.50 ± 0.03	17.50 ± 0.12	17.80 ± 0.10	18.50 ± 0.21	20.33 ± 0.20

notable antibacterial properties, which are superior to those of many traditional antimicrobial agents, including certain plant extracts. Nanomaterials like Ag-NPs have been extensively researched for their ability to combat bacteria by inhibiting their growth and survival [59]. The following factors are part of the mechanism of action: The integrity of the bacterial cell membrane may be compromised by Ag-NPs adhering to the cell surface. The cellular equilibrium may be disturbed by the uncontrollable flow of molecules into and out of the cell as a result of the NPs' increased membrane permeability [60]. Ag-NPs release silver ions (Ag^{+}), which are highly reactive and contribute significantly to their anti-bacterial properties. This can inhibit important cellular procedures, e.g., respiration and cell division [61]. Silver ions can also interrelate with bacterial DNA, producing injury and stopping replication. Ag-NPs can persuade the creation of ROS inside bacterial cells [61,62]. Ag-NPs can penetrate the extracellular polymeric substance (EPS)

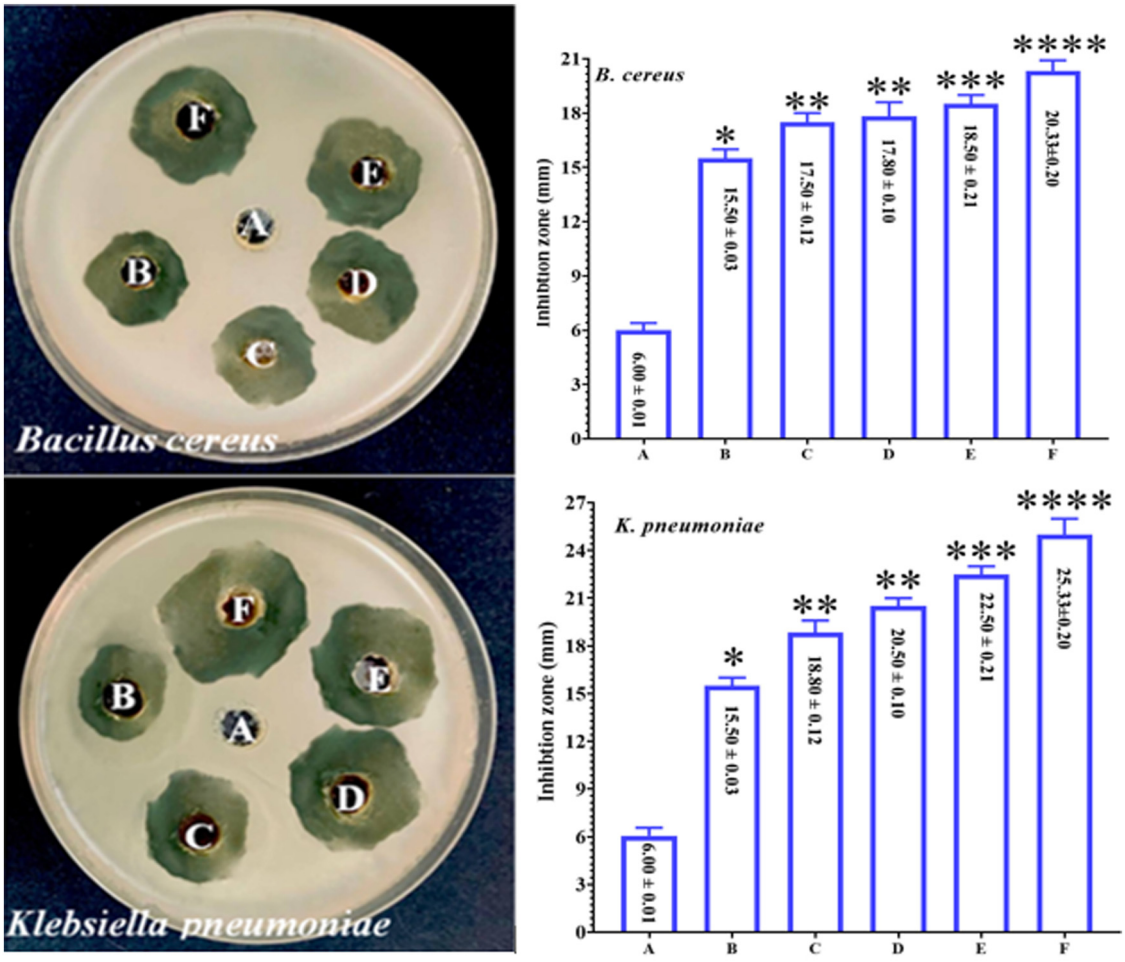

Figure 9: Antibacterial activity of Ag-NPs against *K. pneumoniae* and *B. cereus*. *A* = control, (*B* = 20 μg·mL^{-1}, *C* = 40 μg·mL^{-1}, *D* = 60 μg·mL^{-1}, *E* = 80 μg·mL^{-1}, *F* = 100 μg·mL^{-1}). *P < 0.05, **P < 0.01, ***P < 0.001, ****P < 0.0001.

matrix of biofilms, affecting cell permeability, thus ultimately leading to cell lysis [63,64]. The NPs can work synergistically with other anti-bacterial properties to improve their efficiency [65].

3.4 Antioxidant properties

The antioxidant properties of the ethanolic extract, and Ag-NPs were evaluated by DPPH assay. The results presented that the radical scavenging increased with increasing concentrations for the ethanolic extract and Ag-NPs concentrations at 20, 40, 60, 80 and 100 μg·mL^{-1}. The radical scavenging rate of the ethanolic extract were at 46%, 57%, 67%, 71%, and 77%, respectively. The radical scavenging rate of the Ag-NPs were at 57%, 64%, 77%, 85%, and 88%, respectively, as shown in Figure 10. The results showed that the highest scavenging activity of 88% was obtained for the Ag-NPs at a concentration of 100 μg·mL^{-1}. Ascorbic acid, used as a positive control, displayed strong antioxidant properties and had higher DPPH radical scavenging activity than both the ethanolic extract and Ag-NPs at the same concentration range. The antioxidant actions of the Ag-NPs were measured at 100 μg·mL^{-1}. At room temperature, DPPH is a potent free radical that produces a darkening violet color when it is dissolved in organic solvents. A positive control in the same concentration range, ascorbic acid, was utilized. The antioxidant activity of ethanolic extract or Ag-NPs were concentration dependent, but it remains lower as compared to ascorbic acid alone [37,63,64].

The DPPH free radical scavenging is thought to be involved in the reduction of the stable DPPH radical, which has a characteristic violet color which change to the yellow color. This changing is due to the electron/hydrogen donation from the antioxidant compounds [36]. The presence of phenolic O–H groups and other bioactive compounds in the ethanolic extract, as detected by FTIR, is believed to contribute to the observed antioxidant activity. Ethanolic extract and Ag-NPs were observed to reduce the stability of DPPH, and the violet color altered to yellow due to the occurrence of phenolic O–H groups [23,24]. The DPPH assay is regarded as a reliable, easy and cost-effective technique for assessing the radical scavenging capacity of antioxidants. The idea behind this approach relies on the electron transport responsible for the violet color, when the stable free radicals will react with an antioxidant chemical resulting in electron transfer from the latter compound, which leads to loss of color [36,37]. The results demonstrated that the synthesized Ag-NPs exhibit superior antioxidant activity compared to the ethanolic extract of tangerine peel, as evidenced by the higher DPPH radical scavenging

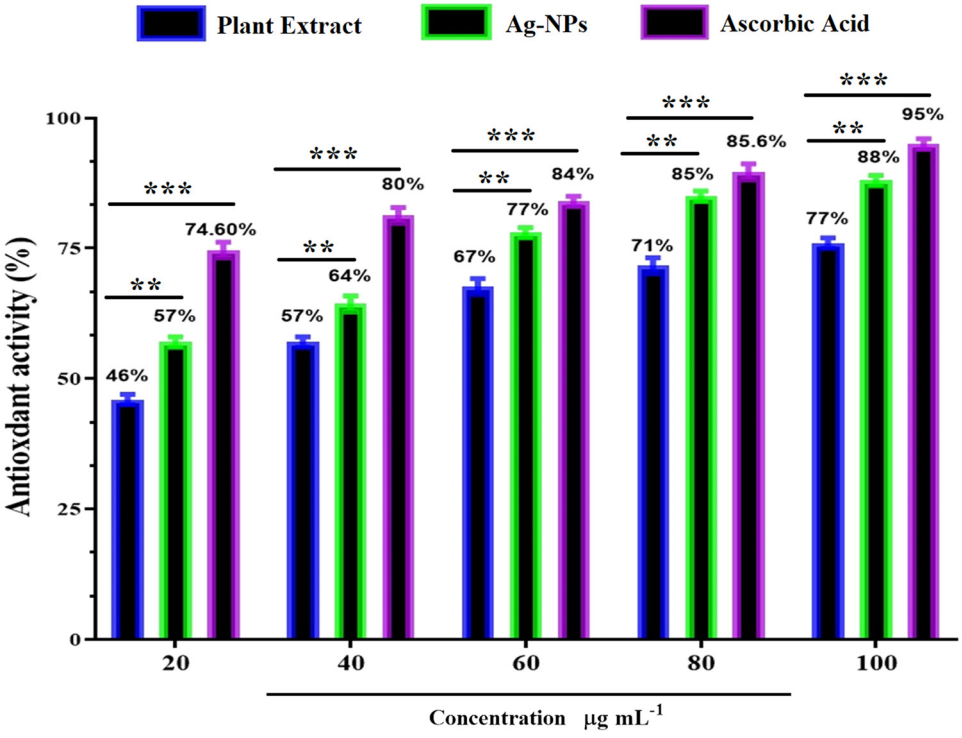

Figure 10: Antioxidant activity of peel extract, Ag-NPs, and ascorbic acid. $^{**}P < 0.01$, $^{***}P < 0.001$.

capacity. The findings highlight the potential of the Ag-NPs as a potent antioxidant agent, which could have valuable applications in various fields, including biomedicine and pharmaceuticals.

3.5 Ag-NPs induce release of LDH

The conversion of lactate to pyruvate, required cellular energy for the synthesis, is regulated by an enzyme called LDH. The cytotoxic properties of plant extract and Ag-NPs on lung tumor cell lines were assessed using LDH. Damaged A549 cells subjected to Ag-NPs release LDH from the cytoplasm, which forms formazan from tetrazolium salt. The percentage of LDH released in dying cells is established through the measurement of production of formazan at a wavelength of 490 nm. Based on the facts obtained, it is possible that Ag-NPs can enter treated cells by penetrating them and causing vesicle growth. Figures 11 and 12 show how the concentration affects the potential for LDH release by plant extract and Ag-NPs. The assays conducted for ethanolic extract peel and Ag-NPs displayed that cytotoxic properties were LDH released proportionally to the concentrations i.e., at concentrations of 12.5, 25, 50, 100, and 200 µg·mL^{-1} of Ag-NPs, the percentage of LDH released in a A549 cells were 8.90%, 28.60%, 42.67%, 68.00%, and 82.53%, respectively. The percentage of LDH released in a A549 cells of the ethanolic extract peel were 6.35%,17.90%, 30.03%, 48.53%, and 76.00%, respectively. The highest percentage of LDH released in the lung was obtained for Ag-NPs. The exact mechanism of how Ag-NPs induce the release of LDH is not completely known or understood yet. However,

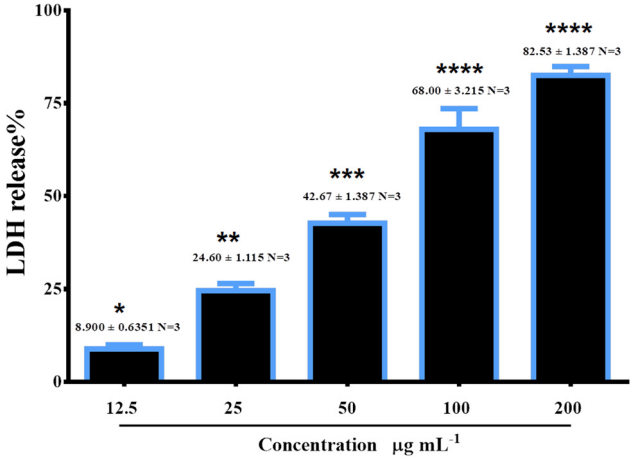

Figure 12: Ag-NPs induces LDH release in A549 cells. *P < 0.05, **P < 0.01, ***P < 0.001, ****P < 0.0001.

several studies have reported that exposure to Ag-NPs can lead to the release of LDH [65–67].

3.5.1 Anticancer activity of Ag-NPs

The anti-proliferative action of the plant extract and Ag-NPs was confirmed to estimate their ability to prevent cell proliferation. The results of the present study established that the treatment of ethanolic extract and Ag-NPs inhibits the development of cancer cells in a dose-dependent way, as seen in Figures 13 and 14. Also, the integration of ethanolic extract and Ag-NPs progresses anti-proliferative result against lung cancer cells. Ag-NPs have special properties that make them principally promising for cancer therapy, for instance, their high surface area to volume ratio and capacity to

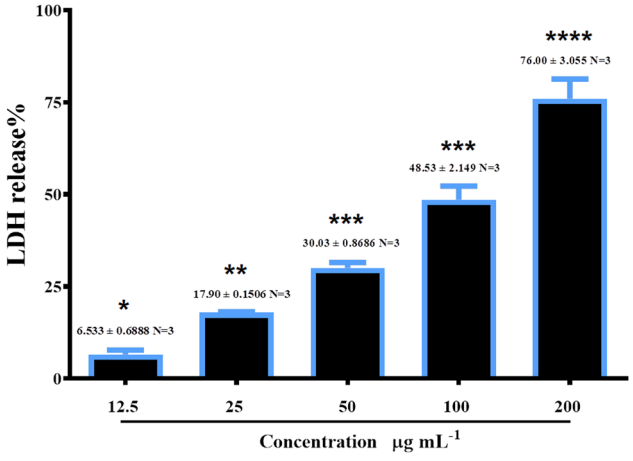

Figure 11: Peel extract induces LDH release in A549 cells. *P < 0.05, **P < 0.01, ***P < 0.001, ****P < 0.0001.

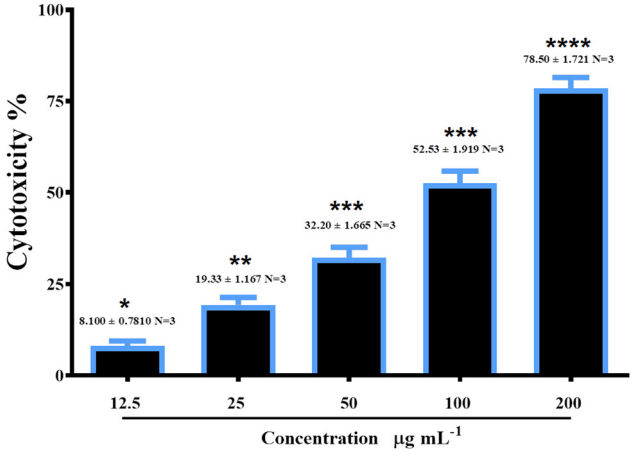

Figure 13: Anti-proliferative properties of peel extract in A549 cells. IC_{50} = 29.36 µg·mL^{-1}. *P < 0.05, **P < 0.01, ***P < 0.001, ****P < 0.0001.

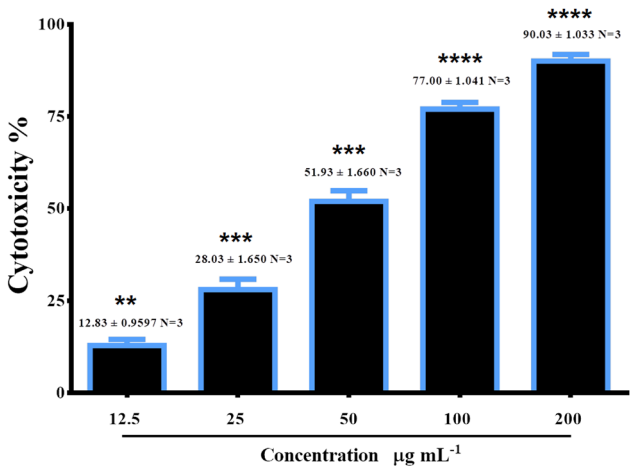

Figure 14: Anti-proliferative properties of Ag-NPs in A549 cells. IC_{50} = 23.91 µg·mL^{-1}. $^{**}P < 0.01$, $^{***}P < 0.001$, $^{****}P < 0.0001$.

penetrate cell membranes. It has been found that the Ag-NPs have anticancer properties in different types of cancer cells via induction of apoptosis, and other mechanisms like drug delivery strategies are developed using hybrid molecular structures, such as Ag-NPs [53,68]. Drug delivery technique based on Ag-NPs now makes it possible to distribute medications like doxorubicin and alendronate inside cancer cells. When administered in this way, the anticancer therapeutic qualities of both medications were demonstrated and improved [69]. Moreover, Ag-NPs' cytotoxicity causes mitochondrial damage in cancer cells. Mitochondrial disturbances related to heterogeneity in regulatory mechanisms include oxidative damage, autophagy, and energy imbalance. Investigation of the harmful effects of Ag-NPs on mitochondria reveals that in A549 and MCF7 cells shows that the role of Ag-NPs interaction disrupts mitochondrial dynamics and biogenesis [70]. There are several advantages of using NPs in the treatment of cancer than those of chemotherapeutic drugs. NPs may be able to further upsurge the delivery of cancer targeted drugs by changing the surface of the NP with typical cancer and tumor cells

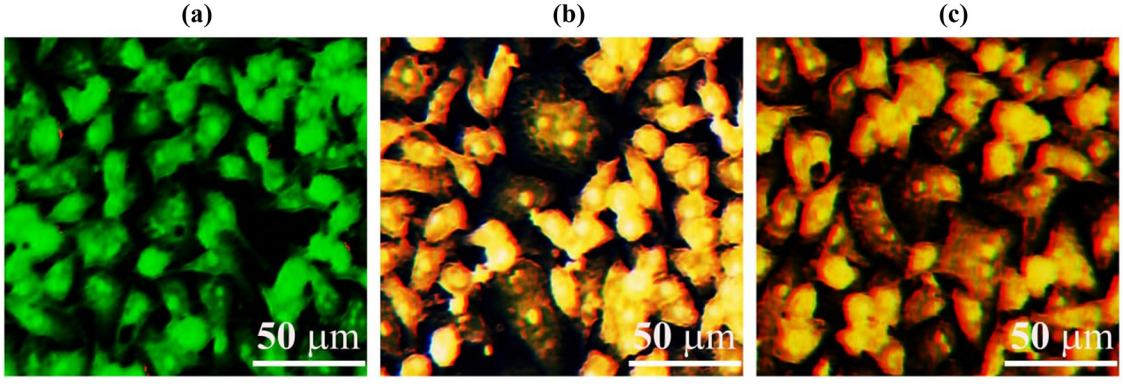

Figure 15: Ag-NPs induces apoptosis in A549 cells. (a) Control cells. (b) A549 cell line after treatment with plant extract, and (c) A549 cell line after treatment with Ag-NPs.

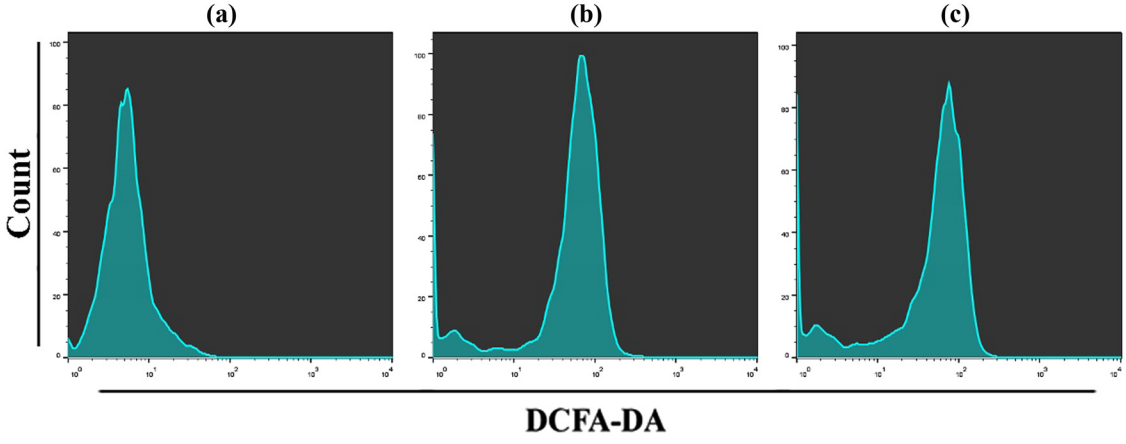

Figure 16: Ag-NPs induces ROS generation in A549. (a) Control cells, (b) extract plant treatment cells, and (c) Ag-NPs treatment cells.

that are focused on ligands. Examples of these ligands include antibodies, biotin, and folic acid. In addition, NPs have the capability to deliver drugs directly to cancer cells and enable prolonged drug release through a variety of mechanisms [52,55]. One example of this is the mixture of a chemotherapeutic drug and a chemo-sensitizer, which produces synergistic anticancer effects [56,57]. Moreover, NPs facilitate the consistency and solubility of therapeutic drugs to obtain site-specific targeting due to their function of enhancing permeability and retention characteristics. The results established that the Ag-NPs have extremely cytotoxic result against A549 cell line than plant extract. The mechanism of act of Ag-NPs any anticancer activity is not completely known but demonstration by [52,53,71]. These potentials make Ag-NPs a promising candidate for the development of effective anticancer therapies.

3.5.2 Ag-NPs induce programmed cell death

The present study proposes that the Ag-NPs can induce programmed cell death of lung cancer cells. The decrease in cell development often includes the change in several significant signaling pathways, which is produced through the induction of a apoptosis mechanism that touches gene expression stages. Furthermore, the nuclear shape of treated cells was assessed by Acridine Orange (AO) and Ethidium Bromide (EB) double staining. Apoptotic cells were assessed based on DNA destruction. In our study, the effectiveness of the plant extract and Ag-NPs was also examined. AO@EB staining was used to study the changed apoptotic features of the nuclear modifications. Non-apoptotic cells seemed green in color, and apoptotic cells seemed orange or red in color subsequent to staining with AO@EB, as shown in Figure 15.

3.5.3 Ag-NPs induce ROS generation in A549 cells

ROS generation is important in cellular signaling pathways, are complicated in signal transduction and sustaining cellular redox homeostasis in aerobic creatures. In addition to being collections of tumors cells, ROS are effective therapeutic agents for the treatment of cancer. In the present investigation, a DCFH DA probe was used to detect the production of intracellular ROS in the A549 cell line. Resulting treatment with Ag-NPs for 24 h, the flowcytometry showed that Ag-NPs importantly increased ROS group as indicated in Figure 16. These findings are in agreement with previous studies [72–74].

4 Conclusion

Successful green synthesis of Ag-NPs as a reducing and capping agent was established using tangerine fruit peel extract. The synthesized Ag-NPs were thoroughly characterized using various analytical techniques, revealing their spherical morphology, nano-scale size range, and chemical composition. The Ag-NPs demonstrated superior antibacterial, antioxidant, and anticancer properties compared to the tangerine peel extract alone. The Ag-NPs induced apoptosis in lung cancer cells (A549) through the generation of ROS, suggesting their potential as an anticancer agent. The potential of Ag-NPs has a powerful antibacterial activity due to their multifaceted mechanisms of action. This study provided a green and environmentally friendly approach for synthesizing Ag-NPs from tangerine fruit peel extract. This research addresses the need for the development of environmentally sustainable and biocompatible nanomaterials, such as Ag-NPs, for various biomedical applications. This offers promising solutions for addressing global health challenges related to communicable diseases and tumor. While the general potentials of Ag-NPs are well-known, the unique characteristics and biological activities of the Ag-NPs synthesized using tangerine peel extract provide new insights and expand the understanding of these nanomaterials. Taken together, AgNPs were used in biomedical applications. So, modern biomedicine's use of nanostructured biomaterials and technologies may consider the use of AgNPs.

Acknowledgements: We would like to acknowledge the University of Technology, Baghdad, for their support. The authors acknowledge Researchers Supporting Project number (RSP-2024R375), King Saud University, Riyadh, Saudi Arabia.

Funding information: Researchers Supporting Project number (RSP-2024R375), King Saud University, Riyadh, Saudi Arabia.

Author contributions: Conceptualization: B.A.A.H., B.S.M., and E.A.M.; methodology: B.A.A.H., B.S.M., E.A.M., M.S.J., and N.N.H.; data curation: M.S.J., K.H.J., N.N.H., and G.M.S.; writing – original draft preparation: B.A.A.H., B.S.M., E.A.M., M.S.J., K.H.J., N.N.H., and G.M.S.; writing – review and editing: B.A.A.H., M.S.J., K.H.J., N.N.H., G.M.S., Y.H.D., and N.M.-D.; validation: BSM, EAM and NM-D; visualization: E.A.M., M.S.J., and K.H.J.; project administration: G.M.S. and Y.H.D. All authors have read and agreed to the published version of the manuscript.

Conflict of interest: Authors state no conflict of interest.

Data availability statement: The datasets generated during and/or analysed during the current study are available from the corresponding author on reasonable request.

References

[1] Ying S, Guan Z, Ofoegbu PC, Clubb P, Rico C, He F, et al. Green synthesis of nanoparticles: Current developments and limitations. Environ Technol Innov. 2022;1:102336.

[2] Hussein NN, Al-Azawi K, Sulaiman GM, Albukhaty S, Al-Majeed RM, Jabir M, et al. Silver-cored Ziziphus Spina-Christi extract-loaded antimicrobial nanosuspension: overcoming multidrug resistance. Nanomedicine. 2023. doi: 10.2217/nnm-2023-0185 C.

[3] Khan I, Saeed K, Khan I. Nanoparticles: Properties, applications and toxicities. Arab J Chem. 2019;12:908–31.

[4] Arshad F, Naikoo GA, Hassan IU, Chava SR, El-Tanani M, Aljabali AA, et al. Bioinspired and green synthesis of silver nanoparticles for medical applications: A green perspective. Appl Biochem Biotechnol. 2024;196:3636–69.

[5] Makarov VV, Love AJ, Sinitsyna OV, Makarova SS, Yaminsky IV, Taliansky ME, et al. "Green" nanotechnologies: synthesis of metal nanoparticles using plants. Acta Nat. 2014;6:35–44.

[6] Husen A, Siddiqi KS. Carbon and fullerene nanomaterials in plant system. J Nanobiotechnol. 2014;12(1):1–10.

[7] Ruban P, SJ LJR, Manickam R, Rathinam R, Rajkumar S, Sharma S, et al. Green synthesis, characterizations, and antibacterial activity of silver nanoparticles from Themeda quadrivalvis, in conjugation with macrolide antibiotics against respiratory pathogens. Rev Adv Mater Sci. 2023;62(1):20220301. doi: 10.1515/rams-2022-0301.

[8] Cozzi R, Ricordy R, Aglitti T, Gatta V, Perticone P, De Salvia R. Ascorbic acid and beta-carotene as modulators of oxidative damage. Carcinogenesis. 1997;18(1):223–8. doi: 10.1093/carcin/18.1.223.

[9] Kang HJ, Chawla SP, Jo C, Kwon JH, Byun MW. Studies on the development of functional powder from citrus peel. Bioresour Technol. 2006;97(4):614–20. doi: 10.1016/j.biortech.2005.03.037.

[10] Zhang QW, Lin LG, Ye WC. Techniques for extraction and isolation of natural products: a comprehensive review. Chin Med. 2018;13:20. doi: 10.1186/s13020-018-0177-x.

[11] Shankar SS, Ahmad A, Sastry M. Geranium leaf assisted biosynthesis of silver nanoparticles. Biotechnol Prog. 2003;19:1627–31. doi: 10.1021/bp034070w.

[12] Singh P, Kim YJ, Wang C, Mathiyalagan R, Yang DC. The development of a green approach for the biosynthesis of silver and gold nanoparticles by using Panax ginseng root extract, and their biological applications. Artif Cell Nanomed Biotechnol. 2016;44:1–8. doi: 10.3109/21691401.2015.1011809.

[13] Singh P, Kim YJ, Yang DC. A strategic approach for rapid synthesis of gold and silver nanoparticles by Panax ginseng leaves. Artif Cell Nanomed Biotechnol. 2016;44:1949–57. doi: 10.3109/21691401.2015.1115410.

[14] Saifuddin N, Wong CW, Nur Yasumira AA. Rapid biosynthesis of silver nanoparticles using culture supernatant of bacteria with microwave irradiation. E-J Chem. 2009;6:61–70.

[15] El Mahdy MM, Eldin TA, Aly HS, Mohammed FF, Shaalan MI. Evaluation of hepatotoxic and genotoxic potential of silver nanoparticles in albino rats. Exp Toxicol Pathol. 2015;67(1):21–9. doi: 10.1016/j.etp.2014.09.005.

[16] Pinzaru I, Coricovac D, Dehelean C, Moacă EA, Mioc M, Baderca F, et al. Stable PEG-coated silver nanoparticles - A comprehensive toxicological profile. Food Chem Toxicol. 2018;111:546–56. doi: 10.1016/j.fct.2017.11.051.

[17] Vandebriel RJ, Tonk ECM, de la Fonteyne-Blankestijn LJ, Gremmer ER, Verharen HW, van der Ven LT, et al. Immunotoxicity of silver nanoparticles in an intravenous 28-day repeated-dose toxicity study in rats. Fibre Toxicol. 2014;11:21. doi: 10.1186/1743-8977-11-21.

[18] Boudreau MD, Imam MS, Paredes AM, Bryant MS, Cunningham CK, Felton RP, et al. Differential effects of silver nanoparticles and silver ions on tissue accumulation, distribution, and toxicity in the Sprague Dawley rat following daily oral gavage administration for 13 weeks. Toxicol Sci. 2016;150:131–60. doi: 10.1093/toxsci/kfv318.

[19] Raies AB, Bajic VB. In silico toxicology: Computational methods for the prediction of chemical toxicity. Wiley Interdiscip Rev Comput Mol Sci. 2016;6:147–72. doi: 10.1002/wcms.1240.

[20] Jackson LK, Futch SH. Osceola Citrus Hybrid: HS180/CH071, rev. 4/2018. EDIS. 2018;3:1–2.

[21] Altammar KA. A review on nanoparticles: characteristics, synthesis, applications, and challenges. Front Microbiol. 2023;14:1155622. doi: 10.3389/fmicb.2023.1155622.

[22] Sharba ZA, Hasoon BA, Maeah RK, Hussein NN. Cytotoxicity, antioxidant, and antimicrobial activities of crude extract of quercus infectoria plant. Plant Arch. 2020;20:227–30.

[23] Al-Saadi HK, Awad HA, Saltan ZS, Hasoon BA, Abdulwahab AI, Al-azawi KF, et al. Antioxidant and antibacterial activities of Allium sativum ethanol extract and silver nanoparticles. Trop J Nat Product Res. 2023;6(7):3105–10. doi: 10.26538/tjnpr/v7i6.5.

[24] Hasan DMA, Hasoon BA, Abdulwahab AI, Jawad KH. Olfactory dysfunction in incidental Lewy body disease and Parkinson's disease: An update. Revis Bionatura. 2022;7(2):19–23. doi: 10.21931/RB/2022.07.02.19.

[25] Vinay CH, Goudanavar P, Acharya A. Development and characterization of pomegranate and orange fruit peel extract based silver nanoparticles. J Manmohan Meml Inst Health Sci. 2018;4(1):72–85.

[26] Minke S, Qihan G, Zhewen X, Sarengaowa S. Recent advances in the health benefits and application of tangerine peel (Citri Reticulatae Pericarpium): A review. Foods. 2024;13(13):1978. doi: 10.3390/foods13131978.

[27] Rafiq S, Kaul R, Sofi SA, Bashir N, Nazir F, Nayik GA. Citrus peel as a source of functional ingredient: A review. J Saudi Soc Agric Sci. 2018;17:351–8. doi: 10.1016/j.jssas.2016.07.006.

[28] Sabry BA, Badr AN, Mohammed DM, Desoukey MA, Farouk A. Validating the protective role of orange and tangerine peel extracts foramending food safety against microorganisms' contamination using molecular docking. Heliyon. 2024;10(6):27737. doi: 10.1016/j.heliyon.2024.e27737.

[29] Saini RK, Ranjit A, Sharma K, Prasad P, Shang X, Gowda KGM, et al. Bioactive Compounds of Citrus Fruits: A Review of Composition and Health Benefits of Carotenoids, Flavonoids, Limonoids, and Terpenes. Antioxidants. 2022;11(2):239. doi: 10.3390/antiox11020239.

[30] Thatyana M, Dube NP, Kemboi D, Manicum AE, Mokgalaka-Fleischmann NS, Tembu JV. Advances in phytonanotechnology: A plant-mediated green synthesis of metal nanoparticles using phyllanthus plant extracts and their antimicrobial and anticancer applications. Nanomaterials. 2023;13(19):2616. doi: 10.3390/nano13192616.

[31] Bora H, Kamle M, Mahato DK, Tiwari P, Kumar P. Citrus essential oils (CEOs) and their applications in food: An overview. Plants. 2020;9:357. doi: 10.3390/plants9030357.

[32] Yosif HM, Hasoon BA, Jabir MS. Laser ablation for synthesis of hydroxyapatite and Au NP conjugated cefuroxime: Evaluation of their effects on the biofilm formation of multidrug resistance Klebsiella pneumonia. J Plasmon. 2023;3:1085–99. doi: 10.1007/s11468-023-02053-y.
[33] Meher A, Tandi A, Moharana S, Chakroborty S, Mohapatra SS, Mondal A, et al. Silver nanoparticle for biomedical applications: A review. Hybrid Adv. 2024;6:100184.
[34] Jawad KH. Laser ablation mediated ZnO nanoparticles inhibit growth and biofilm forming potential of urinary tract bacterium Proteus mirabilis. Adv Nat Sci: Nanosci Nanotechnol. 2023;14(1):015002. doi: 10.1088/2043-6262/aca607.
[35] Sabah T, Jawad KH, Al-Attar N. Synthesis and biomedical activity of aluminium oxide nanoparticles by laser ablation technique. Res J Pharm Technol. 2023;16(3):1267–73.
[36] Mohammed AA, Jawad KH, Çevik S, Sulaiman GM, Albukhaty S, Sasikumar P. Investigating the antimicrobial, antioxidant, and anticancer effects of Elettaria cardamomum seed extract conjugated to green synthesized silver nanoparticles by laser ablation. J Plasmon. 2024;19(3):1187–200. doi: 10.1007/s11468-023-02067-6.
[37] Hasoon BA, Jawad KH, Abdulsahib SS. Synthesis of ciprofloxacin-conjugated gold nanoparticles and their study antibacterial effects on growth biofilm formation through Nebulizer mask against respiratory infection. J Plasmon. 2024;19:1875–89.
[38] Jawad KH, Marzoog TR, Hasoon BA, Sulaiman GM, Jabir MS, Ahmed EM, et al. Antibacterial activity of bismuth oxide nanoparticles compared to amikacin against acinetobacter baumannii and Staphylococcus aureus. J Nanomaterials. 2022;1:8511601.
[39] Jawad KH, Jamagh FK, Sulaiman GM, Hasoon BA, Albukhaty S, Mohammed H, et al. Antibacterial and antibiofilm activities of amikacin-conjugated gold nanoparticles: A promising formulation for contact lens preservation. Inorg Chem Commun. 2024;162:112286.
[40] Mohammed IS, Hammoud D, Alkhazraji SH, Jawad KH, Hasoon BA, Issa AA, et al. Biosynthesized graphene oxide nanoparticles: In-vitro comparative study for biomedical applications. J Plasmon. 2024;1–15. doi: 10.1007/s11468-024-02433-y.
[41] Mahdi LH, Hasoon BA, Sulaiman GM, Mohammed HA, Jawad KH, Al-Dulimi AG, et al. Anti-microbial efficacy of L-glutaminase (EC 3.5.1.2) against multidrug-resistant Pseudomonas aeruginosa infection. J Antibiotics. 2024;77(2):111–9.
[42] Abbas ZS, Sulaiman GM, Jabir MS, Mohammed SA, Khan RA, Mohammed HA, et al. Galangin/β-cyclodextrin inclusion complex as a drug-delivery system for improved solubility and biocompatibility in breast cancer treatment. J Molecules. 2022;27(14):4521.
[43] Ashok K, Usha P, Thotakura R, Kumar NP, Sulaiman GM. Multifunctional characterization and anticancer properties of magnetic zinc ferrite nanoparticles by modified ultrasonic assisted co-precipitation method. ECS J Solid State Sci Technol. 2024;13(8):083011. doi: 10.1149/2162-8777/ad71f2.
[44] Jawad KH, Hasoon BA, Ismail RA, Shaker SS. Preparation of copper oxide nanosheets by pulsed laser ablation in liquid for anticancer, antioxidant, and antibacterial activities. J Indian Chem Soc. 2022;99(11):100773. doi: 10.1016/j.jics.2022.100773.
[45] Al-Salman HNK, Ali ET, Jabir M, Sulaiman GM, Al-Jadaan SA. 2-Benzhydrylsulfinyl-N-hydroxyacetamide-Na extracted from fig as a novel cytotoxic and apoptosis inducer in SKOV-3 and AMJ-13 cell lines via P53 and caspase-8 pathway. Eurpean Food Res Technol. 2020;246:1591–608.
[46] Al-Ziaydi AG, Al-Shammari AM, Hamzah MI, Kadhim HS, Jabir MS. Newcastle disease virus suppress glycolysis pathway and induce breast cancer cells death. Virus Dis. 2020;31(3):341–8.
[47] Al-Musawi S, Albukhaty S, Al-Karagoly H, Sulaiman GM, Jabir M, Naderi-Manesh H. Dextran-coated superparamagnetic nanoparticles modified with folate for targeted drug delivery of camptothecin. Adv Nat Sci: Nanosci Nanotechnol. 2020;11(4):045009.
[48] Sameen AM, Jabir MS, Al-ani MQ. Therapeutic combination of gold nanoparticles and LPS as cytotoxic and apoptosis inducer in breast cancer cells. AIP Conference Proceedings. Vol. 2213, No. 020215, 2020. p. 020215–6. doi: 10.1063/5.0000161.
[49] Mohsin MH, Khashan KS, Sulaiman GM, Mohammed HA, Qureshi KA, Aspatwar A. A novel facile synthesis of metal nitride@metal oxide (BN/Gd_2O_3) nanocomposite and their antibacterial and anticancer activities. Sci Rep. 2023;13(1):22749.
[50] Ibrahim AA, Kareem MM, Al-Noor TH, Al-Muhimeed T, AlObaid AA, Albukhaty S, et al. Pt(II)-thiocarbohydrazone complex as cytotoxic agent and apoptosis inducer in Caov-3 and HT-29 cells through the P53 and caspase-8 pathways. Pharmaceuticals. 2021;14(6):509.
[51] Al Rugaie O, Jabir MS, Mohammed MK, Abbas RH, Ahmed DS, Sulaiman GM, et al. Modification of SWCNTs with hybrid materials ZnO-Ag and ZnO-Au for enhancing bactericidal activity of phagocytic cells against Escherichia coli through NOX2 pathway. Sci Rep. 2022;12(1):17203.
[52] Alsaedi II, Taqi ZJ, Hussien AMA, Sulaiman GM, Jabir MS. Graphene nanoparticles induces apoptosis in MCF-7 cells through mitochondrial damage and NF-KB pathway. Mater Res Express. 2019;6(9):095413.
[53] Fadhil WA, Jabbar II, Ali EH, Sulaiman GM, Khan RA, Mohammed HA. Freshly prepared graphene oxide nanoparticles' wound-healing potential and antibacterial activity specifically against staphylococcus aureus: In vivo efficacy and clinical isolate evaluation. J Plasmon. 2024;1–11. doi: 10.1007/s11468-024-02296-3.
[54] Ashour AA, Raafat D, El-Gowelli HM, El-Kamel AH. Green synthesis of silver nanoparticles using cranberry powder aqueous extract: characterization and antimicrobial properties. Int J Nanomed. 2015;1:7207–21.
[55] Al-Yousef HM, Amina M, Alqahtani AS, Alqahtani MS, Malik A, Hatshan MR, et al. Pollen bee aqueous extract-based synthesis of silver nanoparticles and evaluation of their anti-cancer and antibacterial activities. Processes. 2020;8(5):524.
[56] Vidhu VK, Aromal SA, Philip D. Green synthesis of silver nanoparticles using Macrotyloma uniflorum. Mol Biomol Spectrosc. 2011;83(1):392–7.
[57] Mude N, Ingle A, Gade A, Rai M. Synthesis of silver nanoparticles using callus extract of Carica papaya – a first report. J Plant Biochem Biotechnol. 2009;18:83–6.
[58] Kokila T, Ramesh PS, Geetha DJ. Biosynthesis of silver nanoparticles from Cavendish banana peel extract and its antibacterial and free radical scavenging assay: a novel biological approach. Appl Nanosci. 2015;5:911–20. doi: 10.1007/s13204-015-0401-2.
[59] Srinivasan R, Santhakumari S, Poonguzhali P. Bacterial biofilm inhibition: A focused review on recent therapeutic strategies for combating the biofilm mediated infections. Front Microbiol. 2021;12:12. doi: 10.3389/fmicb.2021.676458.
[60] Stokes JM, Lopatkin AJ, Lobritz MA, Collins JJ. Bacterial metabolism and antibiotic efficacy. Cell Metab. 2019;30:251–9. doi: 10.1016/j.cmet.2019.06.009.
[61] Vinay CH, Goudanavar P, Acharya A. Development and characterization of pomegranate and orange fruit peel extract based silver nanoparticles. J Manmohan Meml Inst Health Sci. 2018;4(1):72–85.

[62] Rafi AA, Mahkam M, Davaran S. The accessible information standard: Action and reaction. Eur J Pharm Sci. 2016;93:64–73.
[63] Hussein NN, Zghair ZM, Hussein RJ, Hameed AZ, Abdul-Jabbar AM, Hasoon BA, et al. Evaluation of the synergistic effects of synthesized silver nanoparticles conjugated tetracycline. Eng Technol J. 2024;42(4):437–445.
[64] Farj AS, AL-Azawi KF. Synthesis, characterization and antimicrobial activity of novel mannich Bases. AIP Conf Proc. 2022;2437:020090.
[65] Hasoon BA, Jawad KH, Mohammed IS, Hussein NN, Al-azawi KF, Jabir MS. Silver nanoparticles conjugated amoxicillin: A promising nano-suspension for overcoming multidrug resistance bacteria and preservation of endotracheal tube. Inorg Chem Commun. 2024;165:112456.
[66] Yosif HM, Hasoon BA, Jabir MS, Yaqoob SH, Samir H, Swelum AA. Antibacterial Activity of Laser Ablated Gold and Hydroxyapatite Nanoparticles Conjugated Cefuroxime against Staphylococcus saprophyticus. Pak Vet J. 2024;44(1):38–46. doi: 10.29261/pakvetj/2024.138.
[67] Gurunathan S, Han JW, Eppakayala V, Jeyaraj M, Kim JH. Cytotoxicity of biologically synthesized silver nanoparticles in MDA-MB-231 human breast cancer cells. BioMed Res Int. 2013;2013:535796.
[68] Jensen SA, Day ES, Ko CH, Hurley LA, Luciano JP, Kouri FM, et al. Spherical nucleic acid nanoparticle conjugates as an RNAi-based therapy for glioblastoma. Sci Transl Med. 2013;5(209):209ra152.
[69] Lee JS, Lytton-Jean AK, Hurst SJ, Mirkin CA. Silver nanoparticle-oligonucleotide conjugates based on DNA with triple cyclic disulfide moieties. Nano Lett. 2007;7(7):2112–5.
[70] Çınar Ayan İ, Güçlü E, Vural H, Dursun HG. Piceatannol induces apoptotic cell death through activation of caspase-dependent pathway and upregulation of ROS-mediated mitochondrial dysfunction in pancreatic cancer cells. Mol Biol Rep. 2022;49(12):11947–57.
[71] Rupa EJ, Nahar J, Al-Amin M, Park JK, Murugesan M, Awais M, et al. Cissus antractica-ZnO NPs induce apoptosis in A549 cells through ROS-generated p53/Bcl-2/Bax signaling pathways and inhibition of inflammatory cytokines. Coatings. 2023;13(12):2077.
[72] Oh SJ, Kim H, Liu Y, Han HK, Kwon K, Chang KH, et al. Incompatibility of silver nanoparticles with lactate dehydrogenase leakage assay for cellular viability test is attributed to protein binding and reactive oxygen species generation. Toxicol Lett. 2014;225(3):422–32.
[73] Liu F, Mahmood M, Xu Y, Watanabe F, Biris AS, Hansen DK, et al. Effects of silver nanoparticles on human and rat embryonic neural stem cells. Front Neurosci. 2015;9:1–9.
[74] Nasrin T, Patra M, Rahaman SM, Das TK, Shaikh S. Biosynthesized CdS nanoparticle induces ROS-dependent apoptosis in human lung cancer cells. Anti-Cancer Agents Med Chem. 2022;22(11):2156–65.